Petroleum Science 21 (2024) 1275–1289

Contents lists available at ScienceDirect

Petroleum Science

journal homepage: www.keaipublishing.com/en/journals/petroleum-science

Original Paper

Micro segment analysis of supercritical methane thermal-hydraulic performance and pseudo-boiling in a PCHE straight channel

Qian Li, Zi-Jie Lin, Liu Yang, Yue Wang, Yue Li, Wei-Hua Cai*

Laboratory of Thermo-Fluid Science and Nuclear Engineering, Northeast Electric Power University, Jilin, 132000, Jilin, China
School of Energy and Power Engineering, Northeast Electric Power University, Jilin, 132000, Jilin, China

ARTICLE INFO

Article history:
Received 1 November 2022
Received in revised form
14 May 2023
Accepted 6 September 2023
Available online 9 September 2023

Edited by Jia-Jia Fei

Keywords:
Printed circuit heat exchanger
Vaporization
Supercritical methane
Pseudo-boiling
Micro segment analysis

ABSTRACT

The printed circuit heat exchanger (PCHE) is receiving wide attention as a new kind of compact heat exchanger and is considered as a promising vaporizer in the LNG process. In this paper, a PCHE straight channel in the length of 500 mm is established, with a semicircular cross section in a diameter of 1.2 mm. Numerical simulation is employed to investigate the flow and heat transfer performance of supercritical methane in the channel. The pseudo-boiling theory is adopted and the liquid-like, two-phase-like, and vapor-like regimes are divided for supercritical methane to analyze the heat transfer and flow features. The results are presented in micro segment to show the local convective heat transfer coefficient and pressure drop. It shows that the convective heat transfer coefficient in segments along the channel has a significant peak feature near the pseudo-critical point and a heat transfer deterioration when the average fluid temperature in the segment is higher than the pseudo-critical point. The reason is explained with the generation of vapor-like film near the channel wall that the peak feature related to a nucleate-boiling-like state and heat transfer deterioration related to a film-boiling-like state. The effects of parameters, including mass flow rate, pressure, and wall heat flux on flow and heat transfer were analyzed. In calculating of the averaged heat transfer coefficient of the whole channel, the traditional method shows significant deviation and the micro segment weighted average method is adopted. The pressure drop can mainly be affected by the mass flux and pressure and little affected by the wall heat flux. The peak of the convective heat transfer coefficient can only form at high mass flux, low wall heat flux, and near critical pressure, in which condition the nucleate-boiling-like state is easier to appear. Moreover, heat transfer deterioration will always appear, since the supercritical flow will finally develop into a film-boiling-like state. So heat transfer deterioration should be taken seriously in the design and safe operation of vaporizer PCHE. The study of this work clarified the local heat transfer and flow feature of supercritical methane in microchannel and contributed to the deep understanding of supercritical methane flow of the vaporization process in PCHE.

1. Introduction

As a high-quality clean energy, natural gas plays a prominent role in more and more fields (Pham et al., 2017). At present, offshore liquefied natural gas (LNG) has become an important way to produce natural gas. One of the main devices for offshore LNG ships is the Floating Storage Regasification Unit (FSRU), which is used to directly vaporize natural gas at sea. Through the heat exchanger on FSRU, liquefied natural gas was heated to near room temperature and access to pipelines on land. In this case, the heat exchanger is the key equipment. However, the traditional heat exchangers, such as plate heat exchangers (Forooghi and Hooman, 2014), spiral heat exchangers (Bes and Roetzel, 1993), and shell-and-tube heat exchangers (Kücük et al., 2019) have some deficiencies as poor pressure capacity, large floor space requirement, and low heat transfer efficiency. The Printed Circuit Heat Exchanger (PCHE) is a new compact microchannel heat exchanger, with atomic diffusion to connect alternately stacked hot and cold plates that have chemically etched small channels. This new type of heat exchanger has the advantages of high temperature and pressure resistance, high thermal efficiency and compactness, and long service life (Huang et al., 2019). It has prominent safety and stability that can

* Corresponding author.
E-mail address: caiwh@neepu.edu.cn (W.-H. Cai).

https://doi.org/10.1016/j.petsci.2023.09.006

effectively prevent the adverse impact caused by ship sloshing. Therefore, the application of PCHE in the vaporization process on FSRU has significant advantages.

The main component of LNG is methane, which is in a transcritical state within the normal operating temperature range of the vaporizer, so its physical properties are variational, which is the difficulty in the current research on the flow and heat transfer characteristics of methane in PCHE (Han et al., 2018; Xu et al., 2016). Currently, supercritical fluid researches show the existence of pseudo-boiling (Xu et al., 2020), referring to the subcritical boiling phenomenon. The effect of pseudo-boiling of supercritical fluid in microchannel heat exchangers is very significant, but the research in this area is still in the initial stage (Yang et al., 2023a, b).

PCHE has been widely applied to many fields including the supercritical carbon dioxide (S–CO_2) Brayton cycle (Nikitin et al., 2006), Very High Temperature Reactor (VHTR) (Katz et al., 2021), Floating Production Storage and Offloading system (FPSO) (Beak et al., 2011), Floating Liquefied Natural Gas Units (Wood and Kulitasa, 2017). The thermal efficiency of PCHE plays a decisive role in the performance of the whole system. Hence, it is important to figure out the thermal-hydraulic characteristics of PCHE in these systems. In the S–CO_2 Brayton cycle, research mainly focuses on thermal-hydraulic performance (Baik et al., 2017; Saeed et al., 2020) and structural optimization (Saeed et al., 2020; Kim et al., 2015). Baik et al. (2017) experimentally investigated the off-design performance of the PCHE and developed the Friction factor and heat transfer correlations. Saeed et al. (2020) carried out a multi-objective optimization research of several fin configurations, and investigated the effect of geometric structure on the performance of the carbon dioxide Brayton cycle. Kim et al. (2015) determined the optimal arrangement of fins in S–CO_2 using a numerical analysis method. Chu et al. (2017) studied the heat transfer characteristics of S–CO_2 in the straight channel PCHE. They found that the performance of S–CO_2 would be greatly improved due to the change of physical properties near the pseudo-critical point. In addition, some researchers investigated the thermal-hydraulic performance of PCHE in the VHTR, and the working fluid was usually helium or S–CO_2. Chen et al. (2019) established a Zigzag channel of PCHE and studied the effects of tortuous curvature radius, channel configuration, and flow direction on the flow and heat transfer performance. They observed that the distribution of helium temperature along the flow direction was approximately linear. Mylavarapu et al. (2014) fabricated two PCHEs for experimental study, and obtained a large number of experimental data of helium gas in PCHE. The correlations between determining the inlet length of the semicircular pipe and pressure drop have been established. Chen et al. (2018) numerical studied the dynamic behavior of a zigzag-channel PCHE, and confirmed its validity by experimental data, providing a reference for the design of an intermediate heat exchanger (IHX). The application of PCHE in FPSO is mainly the liquefaction of natural gas. The temperature of natural gas was decreased from 350 to 380 to 280 K and entered the next stage compressor. In this process, natural gas was in a supercritical state. Cai et al. (2022) numerically studied the thermal-hydraulic performance of supercritical LNG in a Zigzag PCHE used for FPSO, and established new correlations for Fanning friction factor and Nusselt number.

As for PCHE in FSRU, the state of the working fluid is different from that in FPSO. The temperature of LNG is increased from 100 to 150 to about 300 K. In this process, LNG is transcritical flow, in which thermophysical properties have sharp variation around pseudo-critical point. As yet, the research on the flow and heat transfer characteristics of LNG in PCHE is still in its infancy stage. In terms of experimental research, since the main component of LNG is flammable and explosive methane, nitrogen with similar molecular structure is usually used. Zhao et al. (2017a, b) built a PCHE supercritical nitrogen test platform and proposed the relationship between the prediction of straight-channel Nusselt number and Fanning friction factor. Kwon et al. (2018) experimentally studied single-phase, boiling, and condensation heat transfer of supercritical nitrogen in countercurrent structure PCHE. An empirical correlation for PCHE at low temperature is developed. Gu et al. (2013) proposed a semi-empirical correlation for convective heat transfer of supercritical low-temperature methane based on the Probability Density Function (PDF) time-average property. The developed PDF correlation was in good agreement with the experimental data. In terms of numerical simulation, the researchers mainly analyzed the flow and heat transfer characteristics of supercritical methane in PCHE by changing the structural parameters and operating parameters. Kim et al. (Kim et al., 2009; Kim and No, 2011, 2013) studied the thermo-hydraulic characteristics of Zigzag channel PCHE experimentally and numerically. They found that the Zigzag channel had better heat transfer performance than the straight channel, but it would strengthen the flow resistance. Zhao et al. (2019) conducted numerical simulations on Zigzag channel of PCHE and found that Nu/Eu value is higher when the bending angle is less than 15°, at which PCHE has a better heat transfer performance. In addition to the conventional channel shape, Wang et al. (2022) established a PCHE three-dimensional model of sinusoidal channel, and numerically analyzed the heat transfer and pressure drop characteristics of the vaporizer with different amplitudes and wavelengths. Yang et al. (2019) numerically studied the effect of channel cross section on the thermo-hydraulic performance of wavy channel PCHE. The results showed that reducing channel cross section would increase the heat transfer rate and make PCHE more compact. Peng et al. (2020) established single-channel and double-channel PCHE models to simulate the transcritical-condensation flow. They found that the mass flux of condensate flow has a great influence on heat transfer when coupled flow occurs, and the real thermal boundary is mainly composed of condensate flow. Moreover, greater irreversible heat loss will be generated compared with single-phase flow, which provides reference for conjugate heat transfer and design on PCHE. Kim et al. (2016) proposed a mathematical expression in closed form based on a large number of numerical studies, which can be used to predict the thermal performance of cross, parallel, and countercurrent PCHE with semicircular channels.

Supercritical fluid (Yang et al., 2023a, b) was considered as a homogeneous, continuous and single-phase fluid, and the research above was carried out focusing on the single-phase flow of supercritical fluid. However, more and more studies have shown that supercritical fluid can be divided into liquid-like and vapor-like phases based on its properties. Wang et al. (2021) studied the pseudo-boiling phenomenon of supercritical CO_2 and determined the temperature range for pseudo-phase transformation. Licht et al. (2009) studied the flow and heat transfer characteristics of supercritical water. They found that the heat transfer coefficient was enhanced when the temperature was close to the pseudo-critical temperature, and the amplitude of the enhancement depended on the heat flow. Moreover, the heat transfer deterioration phenomenon caused by wall temperature peaks was observed under higher heat flux. Huang et al. (2012) conducted a numerical simulation study on the heat transfer characteristics of supercritical water in a circular tube channel. It was found that heat transfer deterioration occurs in the calculation of various models, and the data obtained by the SST method is in the best agreement with the experimental results. In addition, gravity had an obvious influence on heat transfer deterioration under lower mass flux. Jackson and Hall (1979) found that the buoyancy effect of supercritical water was very significant due to the radial gradient of its density under

lower mass flux, which may lead to heat transfer enhancement or deterioration. Sciortino et al. (1997) studied different states of supercritical fluid through molecular dynamics and drew lines starting from critical points, which are called the Widom lines. Maxim et al. (2019) detected the density fluctuation process of supercritical water from liquid-like to vapor-like when crossing the Widom line through neutron imaging technology. Combined with theory and practice, it proves that the Widom line is indeed the dividing line between the liquid-like region and the vapor-like region. Banuti (2015) proposed a new equation for Widom's pseudo-boiling line, which improved the accuracy. Two limit lines confirm that supercritical boiling takes place within a limited temperature range. The supercritical state not only needs energy to overcome the intermolecular attraction but also needs energy to raise the temperature. The LNG in PCHE used for FRSU is trans-critical flow, and the pseudo-phase transformation phenomenon that happened in this process will have a huge impact on the heat transfer of heat exchanger. Hence, it is essential to conduct further research in this aspect.

In conclusion, the previous numerous studies of PCHE have focused on water, S–CO_2, helium, and nitrogen, and the heat transfer of methane in PCHE was also mainly in a supercritical state. Nevertheless, there are few studies concerned with the heat transfer and pressure drop characteristics the of trans-critical flow of methane in FRSU. In addition, most studies on supercritical methane in PCHE have used the total channel pressure drop and average convective heat transfer coefficient to evaluate the performance of heat exchanger, which ignored the difference of convective heat transfer coefficient in different positions. Especially, the sharp variation of thermophysical properties of the trans-critical process will lead to a large change of the heat transfer performance in the heat exchanger. Therefore, it is essential to figure out the thermal-hydraulic mechanisms of trans-critical flow of methane in PCHE. In this paper, a method of micro-element analysis was adopted to analyze and evaluate the trans-critical local flow and heat transfer characteristics of methane in PCHE based on the numerical simulation results. Combined with the pseudo-boiling theory of supercritical fluid, the temperature boundary between supercritical methane liquid-like and vapor-like was determined. Thus, the influence of vapor-like film on heat transfer of heat exchanger has been studied, which can provide an in-deep understanding of trans-critical flow heat transfer mechanism for optimization design of LNG vaporizer.

2. Numerical method

2.1. Physical model and boundary condition

This paper mainly focuses on the adoption of pseudo-boiling theory to analyze the transcritical flow and heat transfer in the microchannel. Therefore, the physical model employed in the simulation is the most basic semicircle cross section straight channel for PCHE. Namely, a straight channel with a diameter of D_{ch} = 1.2 mm and a length of L = 500 mm is adopted. The heat transfer in solid around the channel is also included in the simulation, with a height of H = 1.3 mm and width of W = 2 mm, and the solid material is 316 L stainless steel. The specific model is shown in Fig. 1.

3D numerical simulation is carried out in a horizontal channel with the effect of gravity included. In considering of the nature gas vaporization process in FSRU, the pressure of methane studied in this paper is 6–9 MPa, and its pseudo-critical temperature is between 190 and 215 K. The inlet boundary condition is mass flux and the outlet boundary condition is constant pressure. Referring to the general requirements of supercritical methane in the PCHE for FSRU, the inlet temperature is 111.15 K, and the temperature variation in the simulation process is within the range of 100–300 K. The wall was set as the second boundary condition in analog with the actual heat transfer conditions between LNG and intermediate medium. The upper and lower walls are set to be constant heat flux boundary condition, and the other walls are set as adiabatic boundary condition.

2.2. Governing equations and solution methods

In this study, CFD software ANSYS Fluent was used to obtain the steady simulation solutions of the supercritical methane flow and heat transfer process. The equations covered in the numerical study are continuity, momentum, and energy equations in supercritical methane flow and heat transfer process as follows:

Continuity equation:

$$\frac{\partial}{\partial x_i}(\rho u_i) = 0 \tag{1}$$

Momentum equation:

$$\frac{\partial(\rho u_i u_j)}{\partial x_j} = -\frac{\partial p}{\partial x_i} + \frac{\partial}{\partial x_j}\left[(\mu+\mu_t)\left(\frac{\partial u_i}{\partial x_j}+\frac{\partial u_j}{\partial x_i}\right) - \frac{2}{3}(\mu+\mu_t)\frac{\partial u_k}{\partial x_k}\right] + \rho g_i \tag{2}$$

Energy equation:

$$\frac{\partial(\rho u_i i)}{\partial x_i} = \frac{\partial}{\partial x_i}\left(\frac{\lambda}{c_p}\frac{\partial i}{\partial x_i}\right) \tag{3}$$

where ρ is density, u_i is the velocity vector, p is pressure, μ and μ_t are the molecular viscosities and turbulent viscosities respectively, i is the enthalpy.

Referring to the simulation work of supercritical fluid flow and heat transfer, it is considered that the SST k-ω turbulence model can show the heat transfer characteristics of supercritical fluids (Kwon et al., 2016; Han et al., 2016; Xu et al., 2014; Li et al., 2011). SIMPLE algorithm was adopted for pressure-velocity coupling solution, and second order upwind was used for pressure discrete scheme. The momentum equation was dispersed by the QUICK scheme, and second order upwind scheme was used for the discretization of energy equation, turbulent kinetic energy equation, and turbulent dissipation rate equation. When the residual value of each equation reached 1.0×10^{-6} and the monitored parameter remains unchanged, the calculation was considered to be converged.

2.3. Thermo-physical properties of supercritical methane

In a large number of experimental studies, it is found that the pressure drop in PCHE is generally within 10%. Therefore, the influences of pressure difference along the channel on the physical properties are ignored. In this case, the physical properties of methane are assumed as a single-valued function of temperature and included in the simulation by means of interpolation within the "piecewise-linear" method of properties in ANSYS Fluent. The pressure of methane in the simulation is 6–9 MPa, which exceeds the critical pressure of methane (P = 4.59 MPa), and methane in the PCHE channel is in a supercritical state. The physical parameters of supercritical methane in this paper were obtained by the NIST database. The thermophysical properties of methane at supercritical pressure change obviously with temperature and have a significant influence on heat transfer when it is close to the pseudo-critical point. Fig. 2 shows the thermal properties of methane at

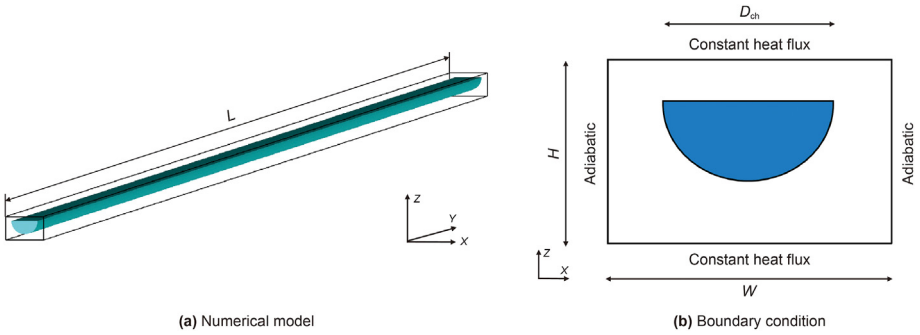

Fig. 1. Numerical model and Boundary condition.

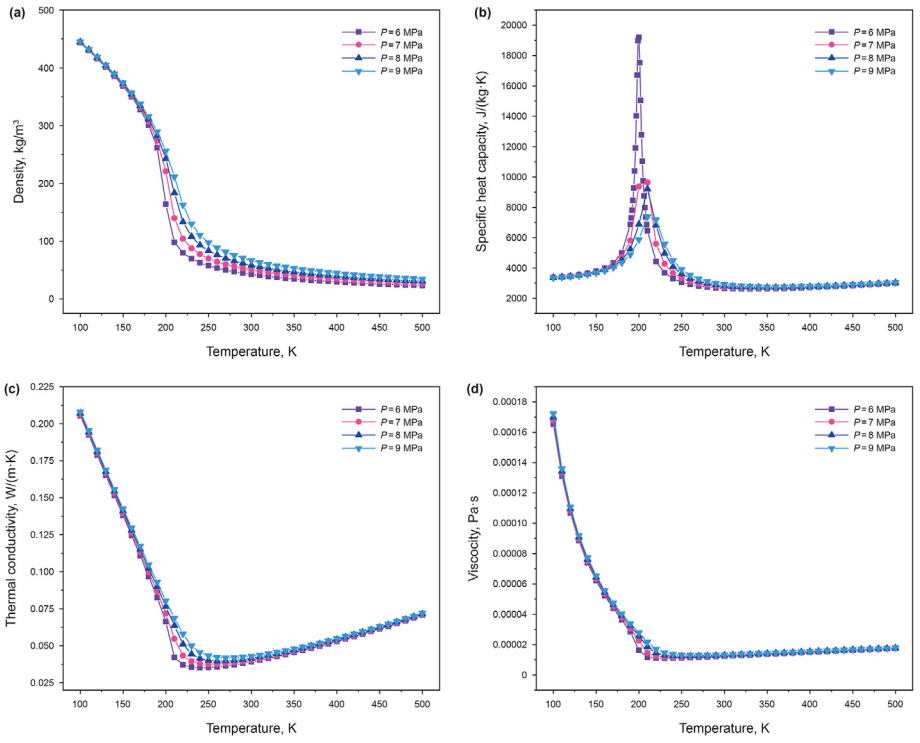

Fig. 2. Thermophysical properties of supercritical methane vary with temperature.

6–9 MPa along with temperature, including density, specific heat capacity, thermal conductivity, and dynamic viscosity. In the numerical simulation, the temperature of supercritical methane ranges from 111.15 to 300 K.

2.4. Grid independence

In the simulation, structured grids were used to divide the simulated fluid domain and solid domain, as shown in Fig. 3. The turbulence model requires a relatively thin grid on the wall to ensure y^+ below 1. So the boundary layer grid is used near the wall, with the height of the first layer grid in 0.003 mm. Guaranteeing the first layer grid height is consistent, six sets of grids with various numbers of grid-point were selected for mesh dependence analysis. The results are shown in Fig. 4 and Table 1, where the relative error is:

$$e = \frac{\varphi_1 - \varphi_{\max}}{\varphi_{\max}} \tag{4}$$

where φ is any parameter that calculates for relative error.

When the number of grids is greater than 1.85 million, the relative error of average outlet temperature and pressure drop is less than 0.5%, indicating that the numerical solution is grid-independent.

2.5. Model validation

In order to ensure the reliability of the numerical method, the experimental study of Zhao et al. was adopted for validation (Zhao et al., 2017a, b). The physical process is supercritical nitrogen flows in a semicircular straight channel, with the diameter of 1.5 mm. Nusselt number *Nu* and Fanning friction factor *f* were used as evaluation indexes. The thermophysical properties of supercritical nitrogen were obtained from the NIST database and included in the simulation by a piecewise polynomial function. The comparison of numerical result and experimental correlation is shown in Fig. 5. The relative error of the Nusselt number is within 11%, and the relative error of the Fanning friction factor is within 16%. In fact, due to the great variation in the physical properties of the simulated supercritical fluid, the simulation error may be larger than that in

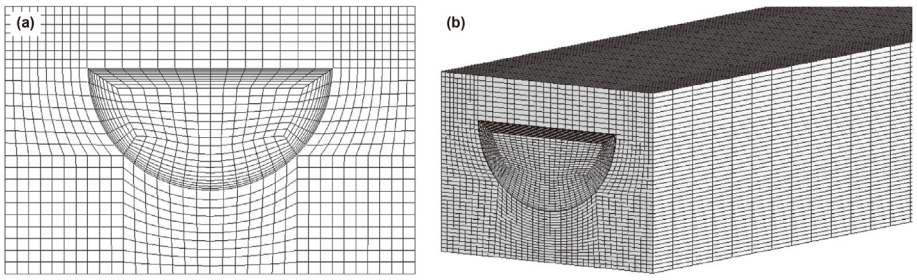

Fig. 3. Mesh of the simulation domain.

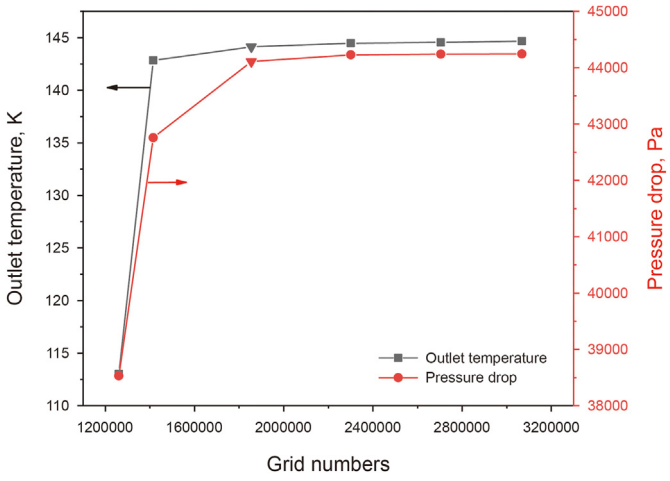

Fig. 4. Grid independence test.

Table 1
Results of grid independency study.

Nodes number, million	1.26	1.41	1.85	2.30	2.70	3.07
Outlet temperature, K	349.46	348.93	348.69	348.47	348.34	348.24
Relative error, %	0.35	0.20	0.13	0.07	0.03	
Pressure drop, Pa	8923	8898	8882	8865	8854	8844
Relative error, %	0.89	0.61	0.43	0.237	0.11	
Wall $y+$	0.42	0.41	0.37	0.36	0.34	0.35

the subcritical fluid. The relative error is acceptable in engineering application. Therefore, the numerical method adopted in this paper is reliable.

2.6. Micro segment analysis method

For the PCHE which consists of plenty of microchannels, the fluid usually flows in relatively separate channels independently. By dividing the channel into micro segments, it is very suitable to establish a one-dimensional mathematical model for the quick calculation of flow and heat transfer characteristics of PCHE. But the one-dimensional mathematical model requires accurate calculation of local flow and heat transfer parameters in the channel. Because the physical properties of supercritical methane vary greatly with temperature in the 500 mm long channel and lead to a significant difference in local convective heat transfer coefficient and pressure drop. It is not accurate to calculate the local flow and heat transfer coefficient in micro segments of the channel with the average value of the whole channel. Therefore, in this paper, the local flow and heat transfer parameters of supercritical methane in the PCHE channel were studied by intercepting micro segments. By obtaining the local flow and heat transfer parameters, data support can be provided for one-dimensional mathematical model calculation and optimization design of PCHE. In the segmentation of channel, the principle is selecting a uniform segment length in keeping the temperature difference between the inlet and outlet of the micro segments less than 1 K. It can ensure the change of methane physical properties in the segment is negligible, so that the local flow and heat transfer parameters can be calculated by taking the average value of the micro segment. The segmentation sketch is shown in Fig. 6.

The convective heat transfer coefficient of each micro segment can be calculated by:

$$h_i = \frac{q_{w,i}}{T_{w,i} - T_{b,i}} \tag{5}$$

where the subscript i represents the value of the i-th segment, $q_{w,i}$ is the heat flux of the inner wall, $T_{w,i}$ is the temperature of the inner

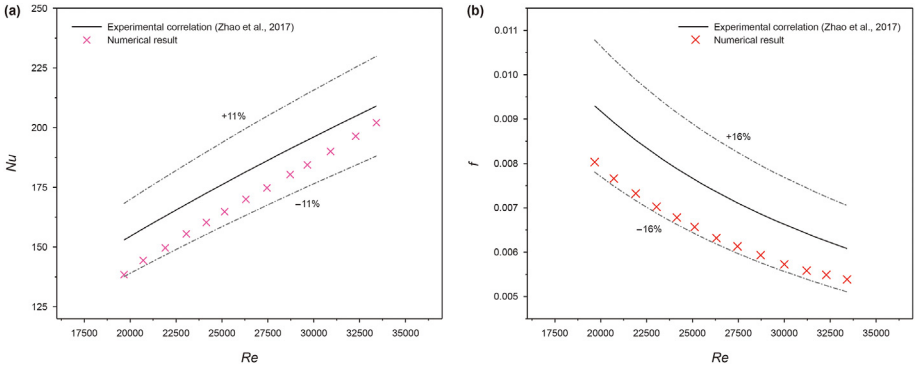

Fig. 5. Nusselt number and Fanning friction factor in experiment study and numerical simulation.

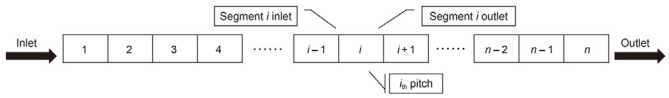

Fig. 6. Sketch of segmentation for PCHE channel.

wall, and $T_{b,i}$ is the average temperature of the working medium.

$$T_{b,\mathrm{i}} = \frac{T_{\mathrm{in},i} + T_{\mathrm{out},i}}{2} \tag{6}$$

The Nusselt number of each micro segment can be calculated by:

$$Nu_i = \frac{h_i D_\mathrm{h}}{\lambda_i} \tag{7}$$

where, h_i is the convective heat transfer coefficient in the i-th segment, D_h is the hydraulic diameter of the channel, and λ_i is the average thermal conductivity coefficient of the fluid in the i-th segment.

The Reynolds number of each micro segment can be calculated by:

$$Re_i = \frac{GD_\mathrm{h}}{\mu_i} \tag{8}$$

where G is the mass flux, and μ_i is the dynamic viscosity of the fluid in the i-th segment.

The Fanning friction coefficient of each micro segment can be calculated by:

$$f_i = \frac{\Delta P_{\mathrm{f},i} D_\mathrm{h}}{2L_i \rho_{\mathrm{b},i} v_{\mathrm{b},i}^2} \tag{9}$$

$$\Delta P_{\mathrm{f},i} = \Delta P_i - \Delta P_{\mathrm{ac},i} \tag{10}$$

$$\Delta P_{\mathrm{ac},i} = \rho_{\mathrm{out},i} v_{\mathrm{out},i}^2 - \rho_{\mathrm{in},i} v_{\mathrm{in},i}^2 \tag{11}$$

where $\Delta P_{\mathrm{f},i}$, $\Delta P_{\mathrm{ac},i}$ are frictional and accelerated pressure drops, L is segment length, $\rho_{\mathrm{b},i}$ is the average density, $v_{\mathrm{b},i}$ is the average flow velocity of fluid in the i-th segment.

3. Results and discussions

In the operation of LNG vaporizer, the inlet and outlet temperature of LNG is almost unchanged, but the flow rate will change according to the user demand, and so will the wall heat flux on the channel wall of PCHE. Therefore, it is necessary to study the flow and heat transfer characteristics of supercritical methane flow in PCHE with different flow rate and wall heat flux. At the same time, since pressure has a significant impact on the flow and heat transfer of supercritical methane in PCHE, the working environment under different pressures must be taken into account. Therefore, this study also simulated the flow of supercritical methane in the channel under different pressures. The simulation cases are as follows.

3.1. Local parameter distribution

At first, in a representative case 4, the temperature and convective heat transfer coefficient along the whole channel is analyzed, as shown in Fig. 7(a). In the segments near the inlet, convective heat transfer coefficient is obviously larger and rapidly decreases to the normal level. This is because the boundary layer of flow near the inlet is in the formation stage and very thin, which makes the heat transfer on the wall very strong. This kind of phenomenon is supposed to be real in PCHE, when fluid from the closure head into the microchannel. When the fluid from a wide area into tiny channels, the Reynolds number will decrease sharply, which means the corresponding boundary layer will significantly get thicker. So, at the entrance of the channels, there will be a formation process of boundary layer. While in the other parts of channel except the inlet region, the temperature increases gradually along the flow direction and the convective heat transfer coefficient shows one obvious peak. After the peak of convective heat transfer coefficient, the temperature slope becomes smaller, due to the significant decrease of convective heat transfer coefficient.

In order to analyze the changes of convective heat transfer coefficient according to fluid physical properties, the distribution of convective heat transfer coefficient with averaged fluid temperature in segments was plotted, as shown in Fig. 7(b). It can be observed that the heat transfer coefficient of supercritical methane in the channel changes significantly with the temperature. In order to explore the reasons for the peaks phenomenon, three characteristic sections are taken, shown as the red dashed lines in Fig. 7(b). They are at the temperature of 185, 200, and 215 K, corresponding to 172, 231, and 322 mm in distance to the inlet, along the axial direction of the channel.

Fig. 8 shows the position and temperature contour of the three sections in the channel. For temperature distribution in the whole channel, the temperature near the wall firstly rises and gradually heats the fluid in the central area of the channel, as the fluid flows from the inlet to the outlet. In each section, there are great temperature differences from area to area with different distances to the wall. The temperature close to the wall is significantly higher than that of the center of the channel, and the temperature gradient is mainly concentrated in the outermost fluid close to the wall.

For the differences between the sections, it can be found that the temperature distribution in the center area of the channel at section a_2 is more uniform, and the temperature gradient is significantly smaller than that of the other two sections. From the point of view of physical properties, the average temperature of section a_2 corresponds to the temperature of the specific heat capacity peak in Fig. 2, which makes the fluid temperature more difficult to change. The larger specific heat capacity is conducive to the fluid transporting heat from the wall in a lower temperature gradient, so that the convective heat transfer coefficient reaches the peak. Downstream from this section, the convective heat transfer coefficient decreases dramatically, corresponding to the specific heat capacity and thermal conductivity decrease with the increase of temperature.

3.2. Pseudo-boiling analysis

According to previous research (Banuti, 2015), the supercritical fluid can be divided into three regimes according to the properties, namely, liquid-like regime, two-phase-like regime, and vapor-like regime. And it is believed that the pseudo-boiling phenomenon exists in the supercritical fluid at a certain temperature. Compare to subcritical fluid that has phase transition in a constant temperature, the supercritical fluid has state transition within a temperature range. As shown in Fig. 9, the three-regime boundaries of supercritical fluid are divided by an onset of pseudo-boiling temperature T^- and a termination of pseudo-boiling temperature T^+. The fluid with the temperature less than T^- is considered as liquid-like regime, with temperature between T^- and T^+ is considered as two-phase-like regime, and with temperature greater than T^+ is considered as vapor-like regime.

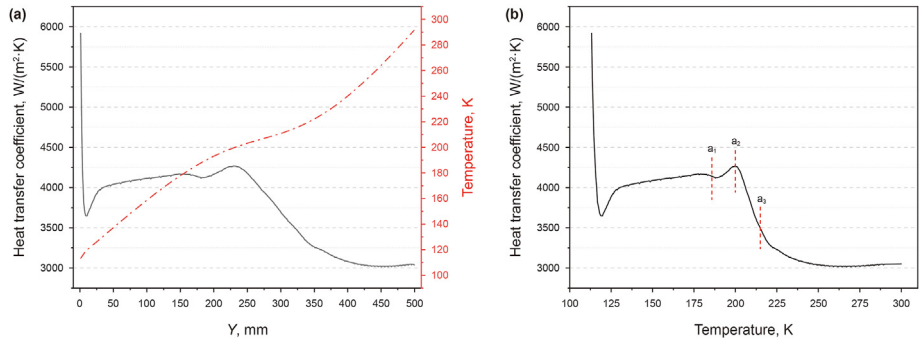

Fig. 7. (**a**) The change of fluid temperature and convective heat transfer coefficient in *Y* direction micro segment of flow passage, (**b**) the change of convective heat transfer coefficient with the mean temperature of fluid in micro-element.

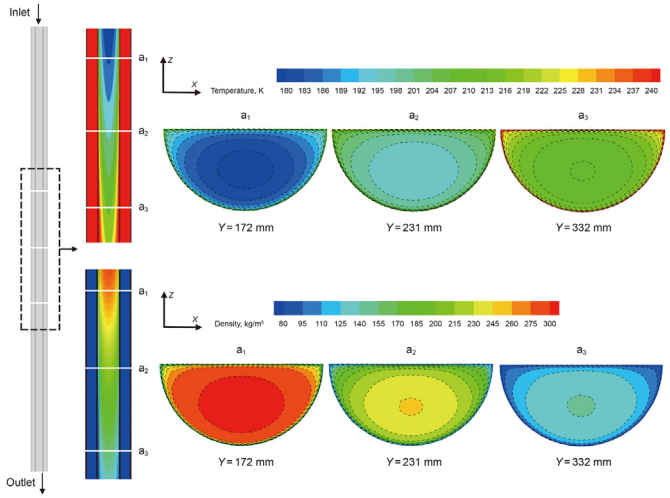

Fig. 8. Temperature and density contours of fluid at different sections.

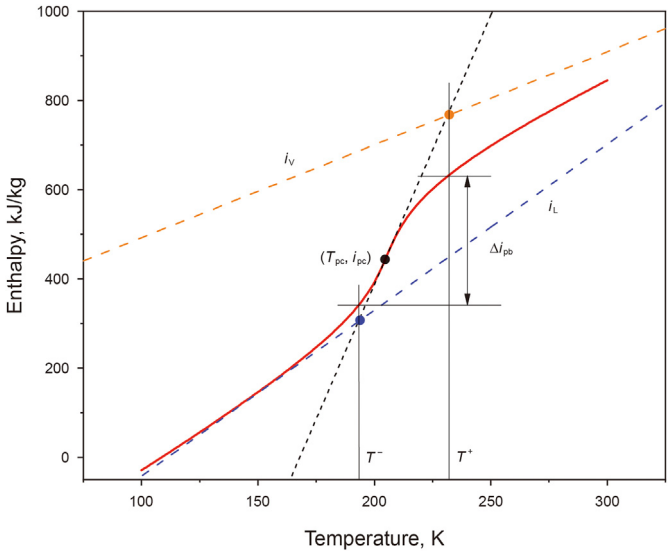

Fig. 9. Calculation scheme for pseudo-boiling temperatures of supercritical methane at 7 MPa.

Based on the physical property of methane provided by the NIST database, the division of three-regime boundaries for supercritical methane is confirmed by enthalpy analysis (Wang et al., 2021). The enthalpy of supercritical methane in the numerical simulation with the pressure of 7 MPa has been analyzed, as shown in Fig. 9. Firstly, tangent lines of the enthalpy-temperature curve are made across pseudo-critical points, and the enthalpy of the two-phase-like regime can be approximately expressed as:

$$i = C_{p,pc}(T - T_{pc}) + i_{pc} \tag{12}$$

where $C_{p,pc}$、 i_{pc} and T_{pc} are the specific heat capacity, enthalpy and temperature at pseudo-critical points, respectively.

The onset of pseudo-boiling temperature T^- and termination of pseudo-boiling temperature T^+ are acquired by the intersection points of two-phase-like regime line with liquid-limit lines and vapor-limit lines, which can be expressed as:

$$i_L = C_{p,L}(T - T_L) + i_{0,L} \tag{13}$$

$$i_V = C_{p,V}(T - T_V) + i_{0,V} \tag{14}$$

where $C_{p.\,L}$, $i_{0,L}$ are the specific heat capacity and initial enthalpy of the fluid at the critical pressure of methane $P = 4.5922$ MPa, respectively. And the parameter $T_L = 0.75\ T_c$, where T_c is the critical temperature of methane (Banuti, 2015). $C_{p,v}$ and $i_{0,V}$ are the specific heat capacity and initial enthalpy of the fluid at $P = 0$ MPa and $T_V = T_c$ in the ideal gas state (Wang et al., 2021).

It can be seen from Fig. 9, when pseudo-boiling occurs, the change of the enthalpy is not as the jump increase in subcritical condition, but in a continuous rising that contains sensible heat and latent heat. So the pseudo-boiling is happened in a certain temperature range of T^- to T^+. The enthalpy difference of the pseudo-boiling can be represented as:

$$\Delta i_{pb} = \int_{T^-}^{T^+} C_p(T)\mathrm{d}T = i(T^+) - i(T^-) \tag{15}$$

Fig. 10 is the schematic diagram of the distribution of phase regimes in the PCHE semicircle channel proposed based on the three-regimes theory. The vapor-like region is covered in the outermost layer with the fluid temperature higher than T^+, the thin layer with the temperature between T^- and T^+ is a two-phase-like region, the innermost layer with the temperature less than T^- is considered as a liquid-like region. With Eqs. (12)–(14), it can be calculated that $T^- = 193.673$ K and $T^+ = 231.749$ K.

In order to present the pseudo-critical boiling phenomenon directly, the obvious convective heat transfer coefficient decline phenomenon occurs after the pseudo-critical point is analyzed, as shown in Fig. 11(a). Three sections A, B, and C are selected along the axis direction, taking an interval of 3 K, with the coordinate value of

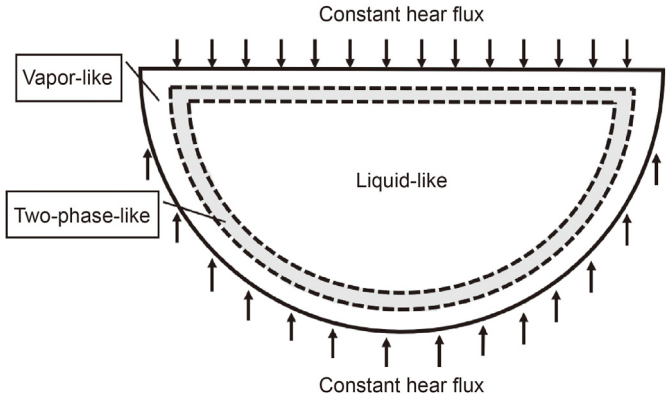

Fig. 10. Phase distribution of supercritical methane in channel.

231, 249, and 267 mm in the channel. Select the center position at the bottom of the arc in the section to present the vapor-like film distribution along the radial direction, according to the T^+ calculated above, as shown in Fig. 11(b). It can be seen that, in section A, the vapor-like film is nascent and in a very thin thickness of 0.0042 mm. While in the next two sections, the thickness of the vapor-like film multiply increases, simultaneous with the increase of temperature in the film. Due to the low density and low thermal conductivity of the vapor-like film, the heat transfer from the wall to the core liquid-like region is seriously blocked, which leads to the convective heat transfer coefficient decreasing sharply.

Fig. 12 shows the temperature contours of the cross sections A, B, and C. The vapor-like films with temperature greater than T^+ are located near the wall, marked as the dotted line. It can be found that the temperature gradient near the wall is large, while that in the internal area of the fluid is small. This situation is similar to the film boiling in the subcritical state that the thin film on the wall caused significant heat transfer deterioration in the channel. Moreover, the fluid temperature in the vapor-like film increased significantly in the downstream sections, indicating that the heat transfer deterioration will be more obvious and the convective heat transfer coefficient will have a significant decrease.

To investigate the development of vapor-like film, three sections D, E, and F, at the end of the downslope, were selected along the *Y*-axis at 318, 332, and 346 mm, also taking an interval of 3 K, as shown in Fig. 13(a). It can be observed from Fig. 13(b) that the vapor-like film thickness increased a lot compared with the first three sections. The vapor-like film thickness is close to half of the radius and most of the area in these sections is in vapor-like regime, as shown in Fig. 14. After the last section F, the vapor-like film is occupied the whole channel and the convective heat transfer coefficient will finally being flatten. Besides, it can be found that, even in the vapor-like film, the temperature gradient near the wall is significantly larger, because there is a flow boundary layer near the wall and the heat is mainly transmitted through heat conduction. The large thermal resistance makes the heat transfer deteriorate significantly near the wall. But the thickness of high temperature gradient area almost keeps the same in sections D, E, and F, which means the thermal resistance of the flow boundary layers in the three sections is equivalent. However, as the fluid moves away from the boundary layer, the turbulent state of the fluid is obviously enhanced and the heat can be better transferred, so that the temperature gradient is significantly reduced.

3.3. Influence of mass flux

In the simulation of cases with different mass flux, the diameter of the channel is 1.2 mm and the heat flux density is 80 kW/m^2, as shown in Table 2. Fig. 15(a) shows the convective heat transfer coefficient distribution of supercritical methane in the straight channel with the temperature of micro segment at different mass flux. The most obvious feature is the convective heat transfer coefficient generally gets larger with the increase of mass flux. This is in accord with the common feature that heat transfer is better at higher Reynolds number. Another feature is, in higher mass flux cases, that there is a more obvious peak of convective heat transfer coefficient located near the pseudo-critical point. But with the decrease of mass flux, the peak gradually disappeared. To investigate the reason for this feature, the iso-surface of termination of pseudo-boiling temperature T^+, which can be regard as the phase interface, in different cases are presented in Fig. 16. As shown in Fig. 16(b) and (c), the phase interface is formed in a macroscopic distance at large mass flux. That means, in the newborn stage of the pseudo-boiling, the vapor-like film partially covered the wall and the heat transfer is much strong like nucleate boiling. When vapor-like film completely covered the wall, the heat transfer is significantly deteriorated like film boiling. While in Fig. 16(a), the formation of the phase interface is in a very short distance at small mass flux, which means the pseudo-boiling becomes film-boiling-like state directly. So there is no convective heat transfer coefficient peak that corresponding to nucleate-boiling-like state in small mass flux cases. Meanwhile, in small mass flux cases, the vapor-like film is formed earlier, which leads to the heat transfer deteriorate appears at lower average fluid temperature, as shown in Fig. 15(a).

For the feature of flow performance, as listed in Fig. 15(b), the local pressure drop in unit length is significantly different with the increase of temperature. It is in a common feature that the pressure drop of the flow in the channel gets increase with the increase of mass flux. While for the unit pressure drop along the channel with

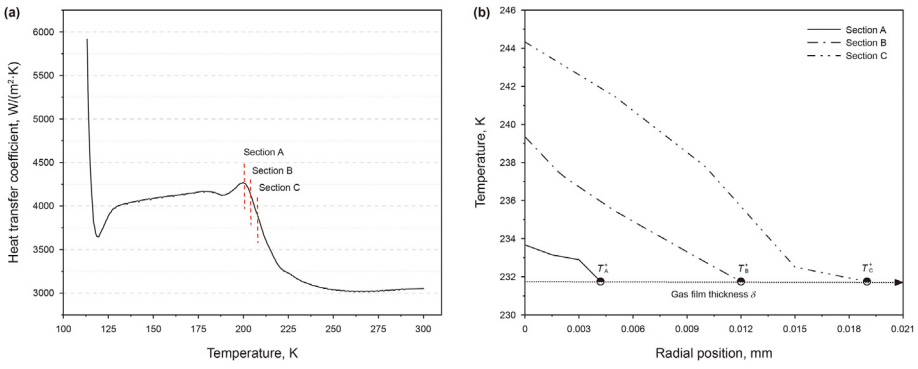

Fig. 11. (**a**) Positions of sections A, B and C, (**b**) thickness of vapor-like film along radial direction.

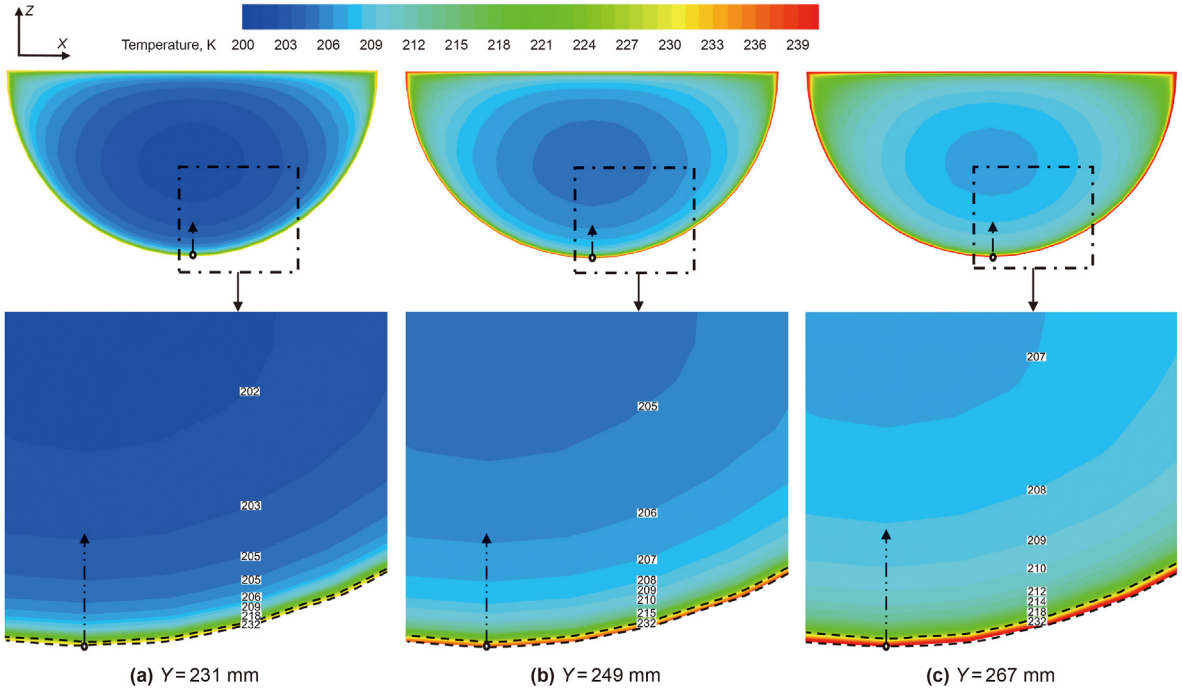

Fig. 12. Temperature distribution in sections A、B and C (dotted line marked the vapor-like region).

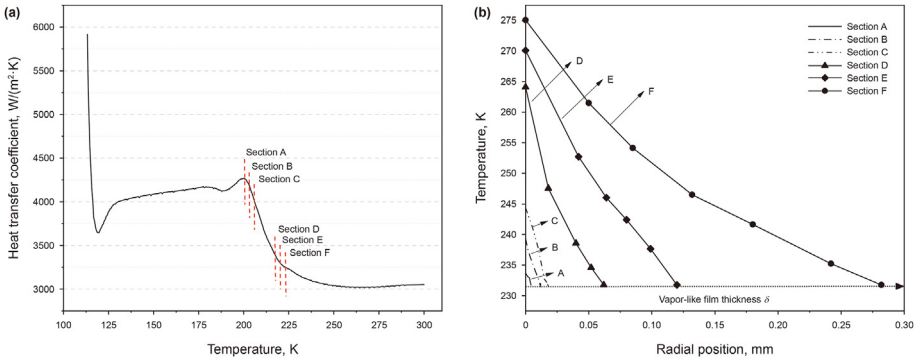

Fig. 13. (**a**) Positions of sections D, E and F, (**b**) thickness of vapor-like film along radial direction.

each mass flux, it is almost in a constant value when the averaged fluid temperature is below the critical point near 200 K. As the averaged fluid temperature is over 200 K, the enlargement of the vapor-like regime area leads to a significant velocity increase that contributes to a significant increase in pressure drop.

To present the averaged heat transfer coefficient and pressure drop of the whole channel, there are two calculating methods. The traditional calculating method of the averaging convective heat transfer coefficient of entire channel is using the inlet, outlet, and wall parameters, as shown in Eqs. (16) and (17):

$$h = \frac{q_w}{T_w - T_b} \tag{16}$$

where, T_w is the average temperature of the channel wall, T_b is the average fluid temperature, and its calculation method is the average temperature of the channel inlet and outlet:

$$T_b = \frac{(T_{in} + T_{out})}{2} \tag{17}$$

The traditional calculating method for pressure drop is:

$$\Delta P = P_{in} - P_{out} \tag{18}$$

where, P_{in} and P_{out} are the pressure of the inlet and outlet.

While according to the numerical simulation results of supercritical methane, the micro segment weighted average calculating method is adopted to obtain the average convective heat transfer coefficient and pressure drop of the channel, as shown in Eqs. (19) and (20):

$$h = \frac{\sum_{i=1}^{n} h_i L_i}{\sum_{i=1}^{n} L_i} \tag{19}$$

$$\Delta P = \sum_{i=1}^{n} \Delta P_i L_i \tag{20}$$

Fig. 17 shows the convective heat transfer coefficient and pressure drop at different mass flux calculated by the micro segment average method and the traditional method. The average pressure

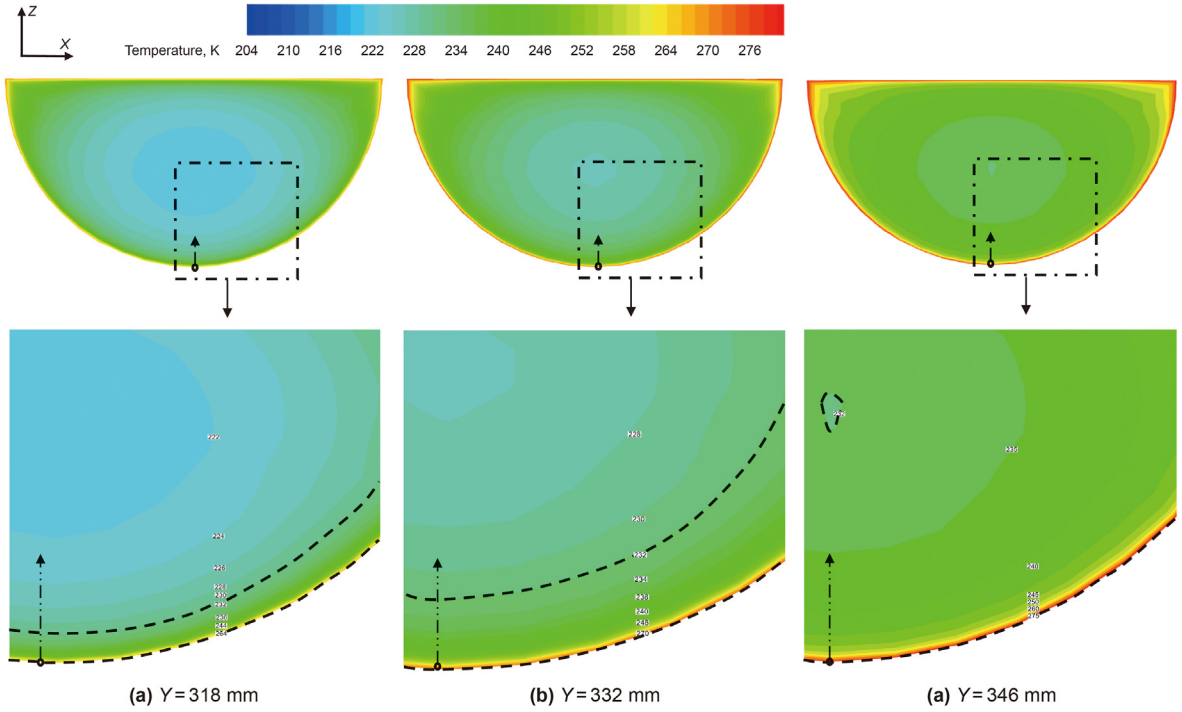

Fig. 14. Temperature distribution in sections D, E, and F (dotted line marked the vapor-like region).

Table 2
Simulation cases.

Case	Mass flux, kg/(m^2·s)	Wall heat flux, kW/m^2	Pressure, MPa
1	200	80	7
2	250	80	7
3	300	80	7
4	350	80	7
5	400	80	7
6	450	80	7
7	400	80	6
8	400	80	8
9	400	80	9
10	300	50	7
11	300	60	7
12	300	70	7
13	300	100	7
14	300	120	7

drop of the two methods are almost the same. But as shown in Fig. 17(a), with the increase of the mass flux, the averaged convective heat transfer coefficient calculated by the micro segment average method is increased, which is consist with the characteristic in Fig. 15(a). While as shown in Fig. 17(b), the averaged convective heat transfer coefficient calculated by the traditional method decreases with the increase of the mass flux, which is contrary to the characteristic in Fig. 15(a). Therefore, the micro segment average method is more accurate to calculate the averaged heat transfer coefficient of the whole channel. It is necessary to analyze the heat transfer characteristics of supercritical flows with drastic changes in physical properties by means of micro segment average.

3.4. Influence of pressure

In the simulation of cases with different pressure, the mass flux is 400 kg/(m^2·s), and the heat flux is 80 kW/m^2, as shown in Table 2. The flow and heat transfer characteristics of supercritical methane under different outlet pressures were studied as shown in Fig. 18(a). When the pressure is closer to the critical pressure, the peak value

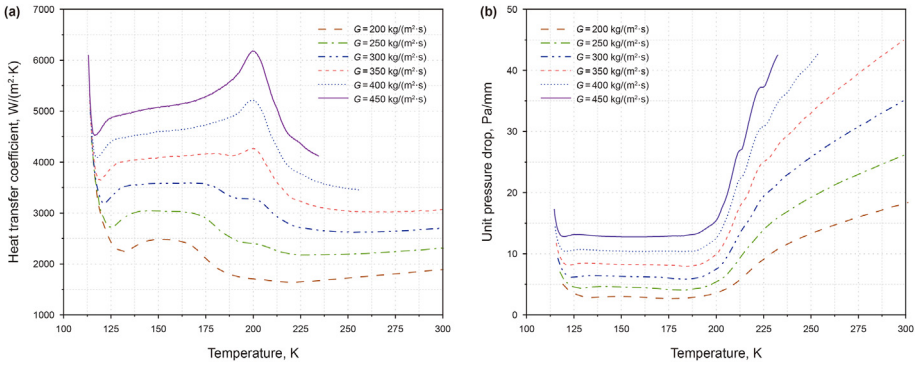

Fig. 15. Convective heat transfer coefficient (**a**) and unit pressure drop (**b**) in segmented channel vary with different mass flux.

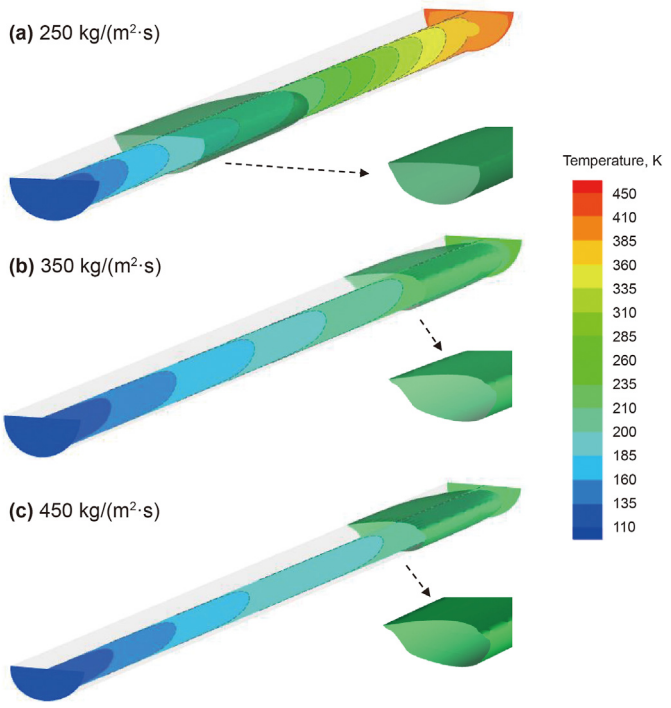

Fig. 16. Temperature distribution in the channel and the iso-surface of termination of pseudo-boiling temperature T^+.

of the convective heat transfer coefficient is higher and then the heat transfer deteriorates more dramatically. This means, when the pressure is closer to the critical pressure, the pseudo-boiling is more remarkable with nucleate boiling and firm boiling features. Even at a pressure far from the critical pressure, the heat transfer deterioration relates to firm boiling feature is still evident. As can be seen from Fig. 18(b), when the fluid average temperature is below the critical point near 200 K, the unit pressure drop is almost independent of the pressure. The reason is the thermophysical properties of fluid are little affected by the pressure, in the liquid-like regime. While in higher temperature, unit pressure drop is increase with the decrease of pressure, which is a common feature for air flow. Because, with the same mass flux, the lower density at lower pressure will lead to a higher velocity and higher pressure drop. In the whole channel, the increase of the outlet pressure result in a decrease of average pressure drop and an increase of average convective heat transfer coefficient, effectively improving the thermal hydraulic performance in the channel, as shown in Fig. 19.

It can be noted that the convective heat transfer coefficient at 6 MPa is significantly higher than that at other pressures. According to the research on this phenomenon in the same way, it is concluded that the vapor-like film production temperature at this pressure is 214.81 K. As can be seen from Fig. 20, when $Y = 355$ mm, the thickness of the vapor-like film is very thin in the region corresponding to the peak value of the convective heat transfer coefficient, and its influence on heat transfer is negligible. In addition, it can be seen from Fig. 2 that methane C_p at 6 MPa is significantly greater than other pressures. A large C_p indicates that the fluid has a larger heat capacity. Subsequently, it can be found that when $Y = 413$ mm, the temperature gradient near the wall increases, and the rapid generation of vapor-like film seriously affects heat transfer. When $Y = 430$ mm, the channel basically becomes a vapor-like fluid, and the heat transfer performance gradually becomes gentle, as shown in Fig. 21.

3.5. Influence of wall heat flux

Fig. 22(a) shows the heat transfer coefficient distribution with different wall heat flux, with the mass flux of 300 kg/(m^2·s) and pressure of 7 MPa, as listed in Table 2. It can be obviously found that the peak of the convective heat transfer coefficient is disappeared in high heat flux cases. This is similar with the low mass flux cases in section 3.3 that when the heat flux is too large, the film-boiling-like state formed quickly and the nucleate-boiling-like state is skipped. Moreover, in the higher heat flux case, the convective heat transfer coefficient is lower on the whole and the heat transfer deterioration in the film-boiling-like state is more serious. The reason is that, when the fluid near the wall is heated at a higher temperature by a larger wall heat flux, the fluid with lower density and smaller thermal conductivity in the flow boundary layer limits the heat transfer from the wall to the central area of the channel. As the flow rate and channel diameter remain unchanged, the average velocity of the fluid at the same temperature is almost the same, so that the wall heat flux has little effect on pressure drop, as shown in Fig. 22(b). In the whole channel, as the heat flux increases, pseudo-boiling occurs earlier, heat transfer deterioration is intensified, and pressure drop increases, as shown in Fig. 23.

4. Conclusion

In this paper, the influences of mass flow rate, pressure, and wall heat flux on the thermo-hydraulic performance of supercritical methane in PCHE were numerically studied. The results are presented in micro segment to show the local convective heat transfer coefficient and pressure drop. Based on the pseudo-boiling theory, the heat transfer and flow features of supercritical methane in the semicircular straight channel are analyzed. The main conclusions are as follows.

For the supercritical methane flow in the microchannel, the local heat transfer coefficient is significantly altered along the

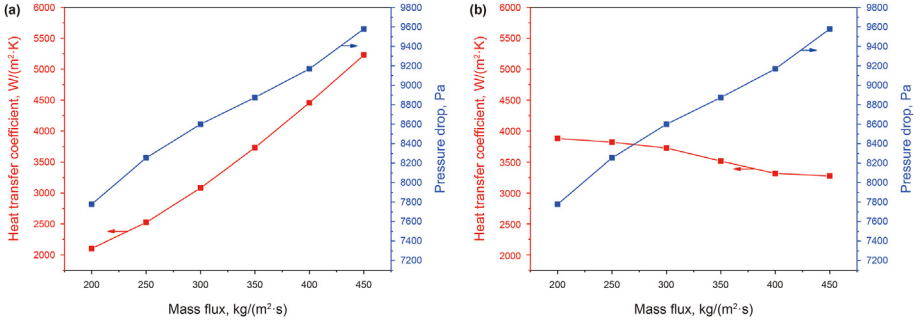

Fig. 17. Average convective heat transfer coefficient vary with different mass flux, (**a**) micro segment average, (**b**) traditional.

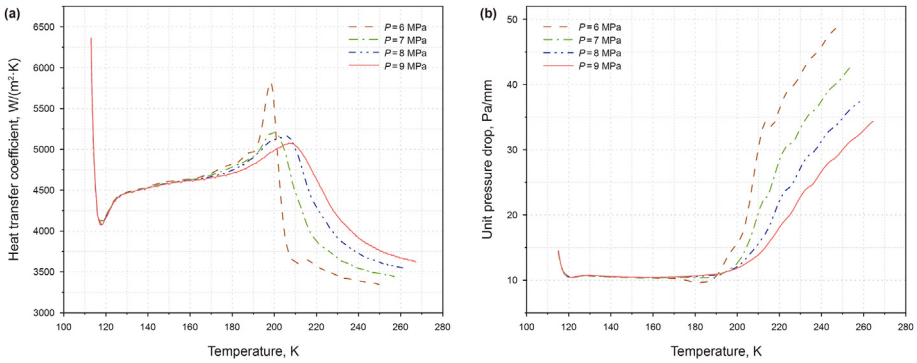

Fig. 18. Convective heat transfer coefficient (**a**) and unit pressure drop (**b**) in segmented channel vary with different pressure.

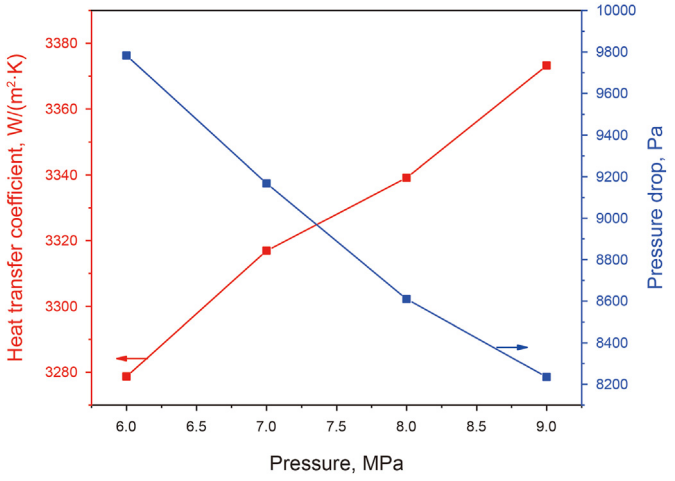

Fig. 19. Average convective heat transfer coefficient and pressure drop vary with different pressure.

channel due to the change of physical properties as the temperature increase along the channel. One peak feature and a following heat transfer deterioration feature of the convective heat transfer coefficient are shown. By analyzing the vapor-like film on the wall, the peak feature and heat transfer deterioration feature of the convective heat transfer coefficient are explained.

The effects of mass flux, pressure, and wall heat flux on heat transfer were analyzed with nucleate boiling and film boiling theory. The nucleate boiling feature can form at high mass flux, low wall heat flux, and near critical pressure, which will result in the peak of the convective heat transfer coefficient. This feature is more remarkable when the pressure close to the critical value. While the film boiling feature will result in a significant heat transfer deterioration. The pressure drop of supercritical methane flow is almost constant when the fluid average temperature is below the critical point and only the mass flux can make a difference in this upstream section. Then pressure drop increases significantly with the rise of fluid average temperature over the critical point that mass flux and pressure have an effect.

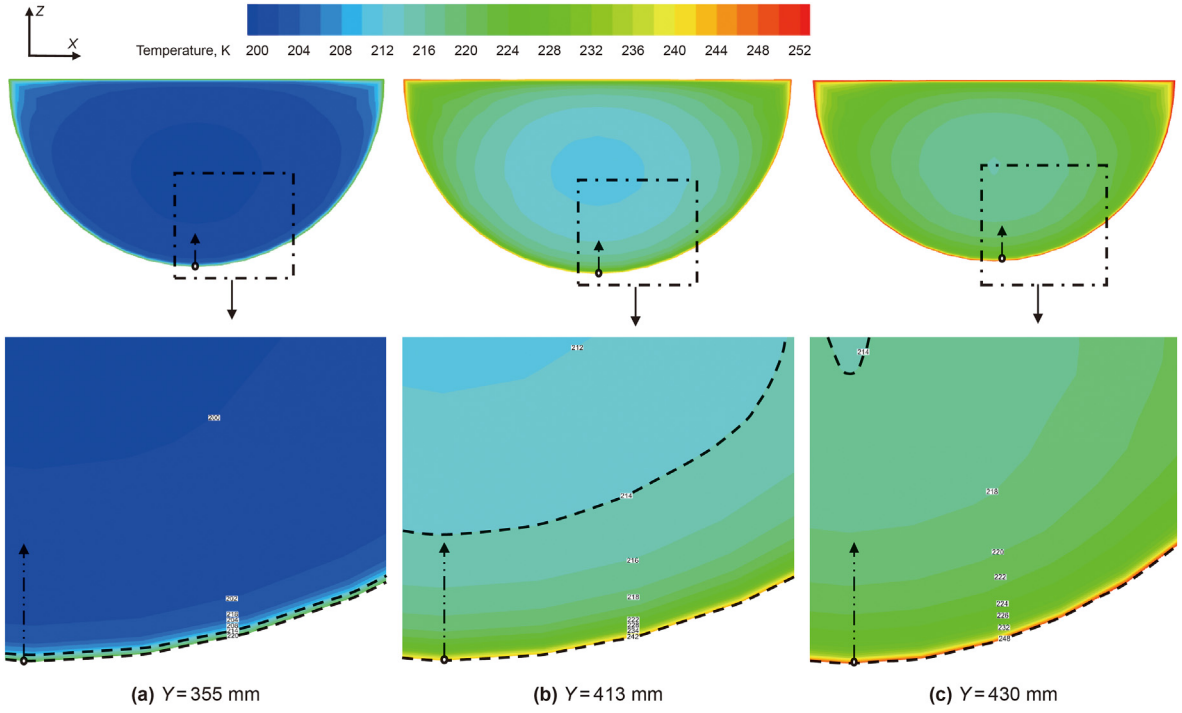

Fig. 20. Temperature distribution in sections A, B, and C (dotted line marked the vapor-like region).

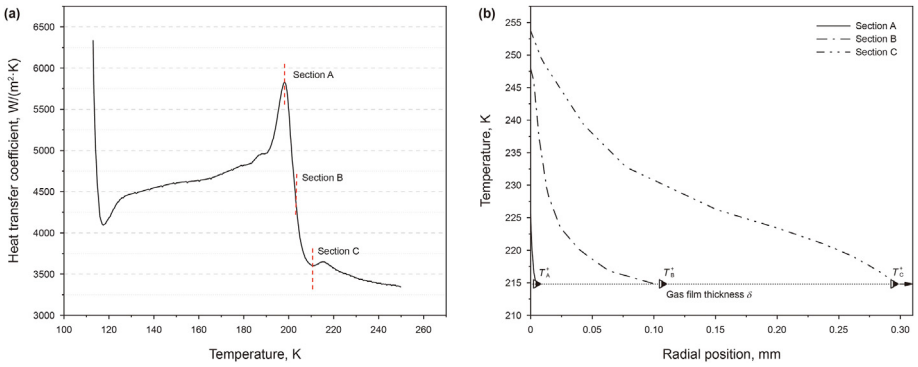

Fig. 21. (**a**) Positions of sections A, B and C, (**b**) thickness of vapor-like film along radial direction.

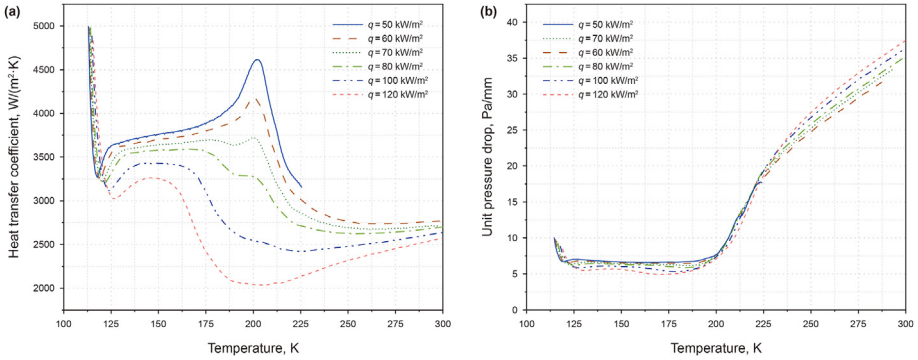

Fig. 22. Convective heat transfer coefficient (**a**) and unit pressure drop (**b**) in segmented channel vary with different wall heat flux.

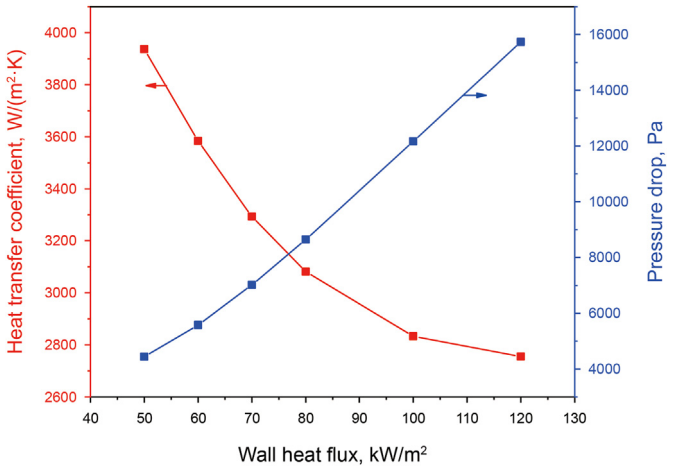

Fig. 23. Average convective heat transfer coefficient and pressure drop vary with different wall heat flux.

In general, the flow and heat transfer phenomenon of critical methane flow in microchannel are abundant and complex. Moreover, the traditional calculating method of averaged heat transfer coefficient of the whole channel cannot acquire the accurate value and the micro segment weighted average calculating method is needed. So the heat transfer deterioration with film-boiling-like state should pay more attention in the design of LNG vaporizer PCHE.

Declaration of competing interest

The authors declare that they have no known competing financial interests or personal relationships that could have appeared to influence the work reported in this paper

Acknowledgement

Financial support for this work was provided by Science and Technology Development Project of Jilin Province (No. 20230101338JC).

Nomenclature

C_p	specific heat capacity
D_h	hydraulic diameter
f	Fanning friction number
G	mass flux
g	gravitational acceleration
h	heat transfer coefficients
L	length
Nu	Nusselt number
P	Pressure
q_w	wall heat transfer rate
Re	Reynolds number
T^+	the termination of pseudo-boiling temperature
T^-	the onset of pseudo-boiling temperature

Greek symbols

Δi_{pb}	pseudo-boiling enthalpy
ΔP	pressure difference
ΔT	temperature difference

λ	thermal conductivity
μ	viscosity
ρ	density
Δ	difference
$\sum$	sum

Subscripts

b	bulk
in	inlet
i	segment *i*th
L	liquid-like
out	outlet
pc	pseudo-critical
pb	pseudo-boiling
V	vapor-like
w	wall

References

Baik, S., Kim, S.G., Lee, J., et al., 2017. Study on CO_2–water printed circuit heat exchanger performance operating under various CO_2 phases for S-CO_2 power cycle application. Appl. Therm. Eng. 113, 1536–1546. https://doi.org/10.1016/j.applthermaleng.2016.11.132.

Banuti, D.T., 2015. Crossing the widom-line-supercritical pseudo-boiling. J. Supercrit. Fluids 98 (3), 12–16. https://doi.org/10.1016/j.supflu.2014.12.019.

Beak, S., Hwang, G., Kim, J., 2011. Development of Compact Heat Exchanger for LNG FPSO. ISOPE, Hawaii, USA.

Bes, T., Roetzel, W., 1993. Thermal theory of the spiral heat exchanger. Int. J. Heat Mass Tran. 36 (3), 765–773. https://doi.org/10.1016/0017-9310(93)80052-V.

Cai, W.H., Li, Y., Li, Q., et al., 2022. Numerical investigation on thermal-hydraulic performance of supercritical LNG in a Zigzag mini-channel of printed circuit heat exchanger. Appl. Therm. Eng. 214 (6), 118760. https://doi.org/10.1016/j.applthermaleng.2022.118760.

Chen, M., Sun, X., Christensen, R.N., 2019. Thermal-hydraulic performance of printed circuit heat exchangers with zigzag flow channels. Int. J. Heat Mass Tran. 130, 356–367. https://doi.org/10.1016/j.ijheatmasstransfer.2018.10.031.

Chen, M., Sun, X., Christensen, R.N., et al., 2018. Dynamic Behavior of a high-temperature printed circuit heat exchanger: numerical modeling and experimental investigation. Appl. Therm. Eng. 135, 246–256. https://doi.org/10.1016/j.applthermaleng.2018.02.051.

Chu, W., Li, X., Ma, T., et al., 2017. Experimental investigation on SCO_2-water heat transfer characteristics in a printed circuit heat exchanger with straight channels. Int. J. Heat Mass Tran. 113, 184–194. https://doi.org/10.1016/j.ijheatmasstransfer.2017.05.059.

Forooghi, P., Hooman, K., 2014. Experimental analysis of heat transfer of supercritical fluids in plate heat exchangers. Int. J. Heat Mass Tran. 74, 448–459. https://doi.org/10.1016/j.ijheatmasstransfer.2014.03.052.

Gu, H., Li, H., Wang, H., et al., 2013. Experimental investigation on convective heat transfer from a horizontal miniature tube to methane at supercritical pressures. Appl. Therm. Eng. 58 (1–2), 490–498. https://doi.org/10.1016/j.applthermaleng.2013.04.049.

Han, C., Ren, J., Dong, W., et al., 2016. Numerical investigation of supercritical LNG convective heat transfer in a horizontal serpentine tube. Cryogenics 78, 1–13. https://doi.org/10.1016/j.cryogenics.2016.05.005.

Han, H., Yan, Y., Wang, S., et al., 2018. Thermal design optimization analysis of an intermediate fluid vaporizer for liquefied natural gas. Appl. Therm. Eng. 129, 329–337. https://doi.org/10.1016/j.applthermaleng.2017.10.043.

Huang, C.Y., Cai, W.H., Wang, Y., et al., 2019. Review on the characteristics of flow and heat transfer in printed circuit heat exchangers. Appl. Therm. Eng. 153 (6), 190–205. https://doi.org/10.1016/j.applthermaleng.2019.02.131.

Huang, Z., Zeng, X., Li, Y., et al., 2012. Model evaluation and numerical analysis of supercritical water heat transfer deterioration in circular tubes. Nucl. Power Eng. 33 (2), 66–70 (in Chinese).

Jackson, J.D., Hall, W.B., 1979. Influence of buoyancy on heat transfer to fluids flowing in vertical tubes under turbulent conditions. In: Turbulent Forced Convection in Channels and Bundles, 2. Hemisphere Publishing Corporation, New York, pp. 613–640.

Katz, A., Aakre, R.S., Anderson, M.H., et al., 2021. Experimental investigation of pressure drop and heat transfer in high temperature supercritical CO_2 and helium in a printed-circuit heat exchanger. Int. J. Heat Mass Tran. 171 (5), 121089. https://doi.org/10.1016/j.ijheatmasstransfer.2021.121089.

Kim, I.H., No, C.H., Lee, J.I., et al., 2009. Thermal hydraulic performance analysis of the printed circuit heat exchanger using a helium test facility and CFD simulations. Nucl. Eng. Des. 239 (11), 2399–2408. https://doi.org/10.1016/j.nucengdes.2009.07.005.

Kim, I.H., No, H.C., 2013. Thermal-hydraulic physical models for a printed circuit heat exchanger covering He, He-CO_2 mixture and water fluids using experimental data and CFD. Exp. Therm. Fluid 48, 213–221. https://doi.org/10.1016/j.expthermflusci.2013.03.003.

Kim, I.H., No, H.C., 2011. Thermal hydraulic performance analysis of a printed circuit heat exchanger using a helium-water test loop and numerical simulations. Appl. Therm. Eng. 31 (17), 4064–4073. https://doi.org/10.1016/j.applthermaleng.2011.08.012.

Kim, T.H., Kwon, J.G., Yoon, S.H., 2015. Numerical analysis of air-foil shaped fin performance in printed circuit heat exchanger in a supercritical carbon dioxide power cycle. Nucl. Eng. Des. 288, 110–118. https://doi.org/10.1016/j.nucengdes.2015.03.013.

Kim, W., Baik, Y., Jeon, D., 2016. A mathematical correlation for predicting the thermal performance of cross, parallel, and counterflow PCHEs. Int. J. Heat Mass Tran. 106, 1294–1302. https://doi.org/10.1016/j.ijheatmasstransfer.2016.10.110.

Kücük, H., Ünverdi, M., Yilmaz, M.S., 2019. Experimental investigation of heat transfer and pressure drop in a mini-channel shell and tube heat exchanger. Int. J. Heat Mass Tran. 55 (4), 1271–1286. https://doi.org/10.1016/j.ijheatmasstransfer.2019.118493.

Kwon, D., Jin, L., Jung, W., et al., 2018. Experimental investigation of heat transfer coefficient of mini-channel PCHE (printed circuit heat exchanger). Cryogenics 92, 19–41. https://doi.org/10.1016/j.cryogenics.2018.03.011.

Kwon, J.G., Kim, T.H., Park, H.S., 2016. Optimization of airfoil-type PCHE for the recuperator of small scale Brayton cycle by costbased objective function. Nucl. Eng. Des. 298, 192–200. https://doi.org/10.1016/j.nucengdes.2015.12.012.

Li, H., Kruizenga, A., Anderson, M., et al., 2011. Development of a new forced convection heat transfer correlation for CO_2 in both heating and cooling modes at supercritical pressures. Int. J. Therm. Sci. 50 (12), 2430–2442. https://doi.org/10.1016/j.ijthermalsci.2011.07.004.

Licht, J., Anderson, M.H., Corradini, M., 2009. Heat transfer and fluid flow characteristics in supercritical pressure water. J. Heat Tran. 131 (7), 98–111. https://doi.org/10.1115/1.3090817.

Maxim, F., Contescu, C., Boillat, P., et al., 2019. Visualization of supercritical water pseudo-boiling at Widom line crossover. Nat. Commun. 10 (1), 1–11. https://doi.org/10.1038/s41467-019-12117-5.

Mylavarapu, S.K., Sun, X., Glosup, R.E., 2014. Patterson thermal hydraulic performance testing of printed circuit heat exchangers in a high-temperature helium test facility. Appl. Therm. Eng. 65 (1–2), 605–614. https://doi.org/10.1016/j.applthermaleng.2014.01.025.

Nikitin, K., Kato, Y., Ngo, L., 2006. Printed circuit heat exchanger thermal–hydraulic performance in supercritical CO_2 experimental loop. Int. J. Refrig. 29 (5), 807–814. https://doi.org/10.1016/j.ijrefrig.2005.11.005.

Peng, Z., Zheng, Q., Chen, J., et al., 2020. Numerical investigation on heat transfer and pressure drop characteristics of coupling transcritical flow and two-phase flow in a printed circuit heat exchanger. Int. J. Heat Mass Tran. 153 (11), 119557. https://doi.org/10.1016/j.ijheatmasstransfer.2020.119557.

Pham, T.N., Long, N.V.D., Lee, M., et al., 2017. Enhancement of single mixed refrigerant natural gas liquefaction process through process knowledge inspired optimization and modification. Appl. Therm. Eng. 110 (5), 1230–1239. https://doi.org/10.1016/j.applthermaleng.2016.09.043.

Saeed, M., Berrouk, A., Siddiqui, M.S., et al., 2020. Effect of printed circuit heat exchanger's different designs on the performance of supercritical carbon dioxide Brayton cycle. Appl. Therm. Eng. 179, 115758. https://doi.org/10.1016/j.applthermaleng.2020.115758.

Sciortino, F., Poole, P.H., Essmann, U., 1997. Line of compressibility maxima in the phase diagram of supercooled water. Phys. Rev. E E. 55 (1), 727–737. https://doi.org/10.1103/PhysRevE.55.727.

Wang, J., Shi, H., Zeng, M., et al., 2022. Investigations on thermal-hydraulic performance and entropy generation characteristics of sinusoidal channeled printed circuit LNG vaporizer. Clean. Technol. Envir. 24 (1), 1–14. https://doi.org/10.1007/s10098-021-02084-1.

Wang, Q., Ma, X., Xu, J., et al., 2021. The three-regime-model for pseudo-boiling in supercritical pressure. Int. J. Heat Mass Tran. 181 (6), 121875. https://doi.org/10.1016/j.ijheatmasstransfer.2021.121875.

Wood, D.A., Kulitasa, M., 2017. A review: optimizing performance of floating storage and regasification units (FSRU) by applying advanced LNG tank pressure management strategies. Int. J. Energy Res. 42 (6), 1–28. https://doi.org/10.1002/er.3883.

Xu, J., Zhang, H., Zhu, B., et al., 2020. Critical supercritical-boiling-number to determine the onset of heat transfer deterioration for supercritical fluids. Sol. Energy 195 (8), 27–36. https://doi.org/10.1016/j.solener.2019.11.036.

Xu, S., Chen, X., Fan, Z., 2016. Thermal design of intermediate fluid vaporizer for subcritical liquefied natural gas. J. Nat. Gas Sci. Eng. 32, 10–19. https://doi.org/10.1016/j.jngse.2016.04.031.

Xu, X., Ma, T., Li, L., 2014. Optimization of fin arrangement and channel configuration in an airfoil fin PCHE for supercritical CO_2 cycle. Appl. Therm. Eng. 70 (1), 867–875. https://doi.org/10.1016/j.applthermaleng.2014.05.040.

Yang, G., Zhang, W.C., Binama, M., et al., 2023a. Review on bubble dynamic of subcooled flow boiling-part a: research methodologies. Int. J. Therm. Sci. 184 (2), 108019. https://doi.org/10.1016/j.ijthermalsci.2022.108019.

Yang, G., Zhang, W.C., Binama, M., et al., 2023b. Review on bubble dynamic of subcooled flow boiling-part b: behavior and models. Int. J. Therm. Sci. 184 (2), 108026. https://doi.org/10.1016/j.ijthermalsci.2022.108026.

Yang, Y., Li, H., Yao, M., et al., 2019. Investigation on the effects of narrowed channel cross-sections on the heat transfer performance of a wavy-channeled PCHE. Int. J. Heat Mass Tran. 135 (13), 33–43. https://doi.org/10.1016/j.ijheatmasstransfer.2019.01.044.

Zhao, Z., Zhang, X., Zhao, K., 2017a. Numerical investigation on heat transfer and flow characteristics of supercritical nitrogen in a straight channel of printed

circuit heat exchanger. Appl. Therm. Eng. 126, 717–729. https://doi.org/10.1016/j.applthermaleng.2017.07.193.
Zhao, Z., Zhang, X., Zhao, K., et al., 2017b. Numerical investigation on heat transfer and flow characteristics of supercritical nitrogen in a straight channel of printed circuit heat exchanger. Appl. Therm. Eng. 126, 717–729. https://doi.org/10.1016/j.applthermaleng.2017.07.193.
Zhao, Z., Zhou, Y., Ma, X., 2019. Numerical study on thermal hydraulic performance of supercritical LNG in Zigzag-type channel PCHEs. Energies 12 (3), 1–19. https://doi.org/10.3390/en12030548.